Iranian Journal of Oil & Gas Science and Technology, Vol. 7 (2018), No. 4, pp. 59-78
http://ijogst.put.ac.ir

Numerical Investigation of the Impact of Inlet Channel Numbers on the Flow Pattern, Performance, and Erosion of Gas-particle Cyclone

Seyed Masoud Vahedi[1], Farzad Parvaz[2,*], Mohammad Kamali[3], and Hasti Jafari Jebeli[1]

[1] M.S.Student, Department of Mechanical Engineering, Semnan University, Semnan, Iran
[2] PhD Candidate, Department of Mechanical Engineering, Behbahan Branch, Islamic Azad University, Khuzestan, Iran
[3] M.S.Student, Department of Mechanical Engineering, Najafabad Branch, Islamic Azad University, Isfahan, Iran

Received: January 05, 2018; *revised*: January 14, 2018; *accepted*: January 28, 2018

Abstract

The effect of adding extra inlet channels on the operation of the Stairmand Cyclone has been investigated numerically. The Reynolds stress model (RSM) and Eulerian-Lagrangian method were used to investigate the complex turbulent flow and cyclone performance. The impacts of one-way coupling and two-way coupling models on the cyclone efficiency and the calculation of cut-off size diameter were examined. The results showed that a rise in channel number increases the tangential velocity and extends the Rankine vortex region. Moreover, in the four-inlet cyclone, the direction of flow changes unlike the one-inlet and two-inlet cyclones, and it behaves like a jet flow. According to the results, the collection efficiency and cut-off size diameter of the four-inlet cyclone are respectively about 10.78% higher and 35% lower than those of one-inlet configuration. Therefore, the performance of four-inlet cyclone is the highest among the three investigated configurations due to high tangential and axial velocities. A cyclone with more inlets has a more symmetrical flow pattern. Consequently, the four-inlet cyclone has the lowest flux of erosion among the others. The results of cyclone performance reveal a slight difference between one-way coupling and two-way coupling models.

Keywords: Number of Inlet Channels, Reynolds Stress Model (RSM), Two-way Coupling Model, Eulerian-Lagrangian Method, Erosion Modeling

1. Introduction

Despite its simple geometry, cyclones have a very complicated flow dynamics to separate particles. Centrifugal and gravitational are the two main forces used by this industrial device for the separation of particles from the flow. There are many types of cyclones used in various industries, but the most famous and practical one is Stairmand used in petroleum and food industries as well as gas and petrochemical applications (Demir et al., 2016; Vahedi et al., 2017b; Mothes and Löffler, 1988). The two-phase flow of particles and gas enters the cyclone tangentially through the cyclone inlet creating two vortexes in the cyclone. One causes the flow to swirl upward and exits through the vortex finder, while the other one swirls downward and transfers the particles towards cyclone walls and the dustbin at the bottom of the cyclone, where they are collected (Hosseini et al., 2015).

Cyclone efficiency has motivated many researchers to study the performance of this device presenting mathematical models originated from experimental data (Mothes and Löffler, 1988; Iozia and Leith, 1990; Avci and Karagoz, 2003). For the typical Stairmand cyclone, the inside flow is three

* Corresponding Author:
Email: jf.parvaz@semnan.ac.ir

dimensional, swirling, anisotropic, and complex, so the results of CFD simulations considerably depend on modeling and choosing the appropriate turbulent model (Avci and Karagoz, 2003; Kaya and Karagoz, 2009; Griffiths and Boysan, 1996; Hoekstra, 2000). Kaya and Karagoz (2009) used Reynolds stress modeling (RSM) to simulate swirling flow inside the gas cyclone three-dimensionally. Their results revealed that the dipleg length influences the cyclone efficiency more than pressure drop especially at lower inlet velocities. Another investigation was carried out by Griffiths and Boysan (1996) in which they utilized an empirical theory to investigate the cyclone performance; their CFD results well suited experimental data. Works done by Griffiths and Boysan (1996) and Kaya and Karagoz (2009) showed an anisotropic and turbulent rotating flow inside the cyclone. According to their studies, the accuracy in choosing the turbulent models and correct assumptions affect the numerical results remarkably. The k-ε, RNG k-ε, and RSM turbulent models were used by Hoekstra (2000) and Chuah et al. (2006) to study the gas-particle cyclones. Their outcomes indicated that RSM model explains the flow behavior inside the cyclone better than the others; hence, it was preferred to be used by many researchers. According to linearity in the Boussinesq hypothesis, k-ε is not capable of estimating the anisotropic turbulent stress since it only involves turbulent kinetic energy and dissipation terms. Wang et al. (2017) investigated the gas-oil cyclone, and studied the impacts of droplets collision, breakup, and droplet-wall collisions; they concluded that there was good agreement between experimental data and the results of RSM turbulent model. Khosravi Nikou and Ehsani (2008) investigated the ability of k-ε, RNG k-ε, k-ω, and BSL turbulent models in the CFD simulation of heat and mass transfer and the hydrodynamics of a two-phase flow through a Flexipac1Y structured packing. They compared their study results with the experimental data and concluded that k-ε and RNG k-ε are not accurate models for complex flows.

The shape of two vortexes relies on many factors like geometric parameters, surface roughness, particle/droplet diameter, and operational conditions. The effects of three distinct values of wall roughness, alongside different droplet sizes and various gas inlet velocities on the flow parameters have been studied by Vahedi et al. (2017b). Their results showed that an increase in surface roughness leads to a decline in tangential velocity as the flow resistance rises. Vahedi et al. (2017a) numerically studied the impact of the conical section on the flow pattern and cyclone performance by comparing the results of a dual-cone cyclone with those of a single-cone cyclone. They reported that tangential velocity and Rankine vortex region decrease when the separation part space is decreased. Also, a smaller outlet section and less space for particle movement resulted from adding another cone lead to an increase in cyclone efficiency. Brar et al. (2015a) conducted a numerical study on the impacts of cylinder length and cone length on the Stairmand cyclone; they concluded that increasing the cylinder length from 1D to 5.5D decreases the pressure drop by 34%, whereas the cyclone efficiency rises by almost 9.5%. Increasing cone length by 6.5 times resulted in an increase of 29% and 11% in pressure drop and cyclone efficiency respectively. Gao et al. (2013a) studied the effects of central channel dimensions on the performance of gas-oil cyclone and showed that the pressure drop increases by a decrease in central channel diameter. The tangential velocity near the wall is about 0.8 to 1 times of inlet velocity, while the figure for the maximum tangential velocity is almost 1.8 to 2 times of inlet velocity. Azadi et al. (2010) used the RSM turbulent model and Eulerian-Lagrangian approach to tracking the particle paths in several gas-particle cyclones. They concluded that an increase in the size of the cyclone would grow the cut-off size diameter and pressure drop. Karagoz et al. (2013) studied a new type of cyclone by using RSM turbulent model to simulate the continuous phase. They showed that increasing the length and diameter of the vortex limiter would lead to decrease in cut-off size diameter, which results in an increase in collection efficiency. Elsayed and Lacore (2012) numerically studied four different geometries of dust outlet, namely without dustbin, with dustbin, with dipleg and with dustbin plus dipleg. All the four configurations had almost an equal maximum velocity.

However, three of them, i.e. without dustbin, with dipleg and with dustbin plus dipleg, exhibited an M-shape axial velocity profile, but the one with dustbin produced an inverted V-shape axial velocity profile. Brar et al (2015b) investigated the impact of varying diameters on the pressure drop, collection efficiency, and cut-off diameter of the cyclone. They revealed that an increase in cyclone diameter increases the collection efficiency at the expense of increasing pressure drops across the gas cyclones. Zhao et al. (2006) considered two cyclones with two different inlet channels numerically. The first cyclone had a typical inlet channel, whereas the second one had a curvature at the end of its inlet channel. They claimed that this curvature accounted for a more symmetrical flow pattern and better efficiency compared to a typical cyclone. According to their study, the geometrical changes affect the flow pattern, particle separation, and cyclone efficiency. Therefore, according to the above literature review, it can be concluded that, in order to achieve a higher efficiency, the geometrical study of the cyclone is inevitable.

In the current study, the effect of increasing inlet channel numbers at a constant total volumetric mass flow rate on the flow pattern and the efficiency of the Stairmand cyclone is studied. To this end, the effect of inlet channel numbers on velocity and pressure distributions is examined for one-inlet, two-inlet, and four-inlet configurations by using RSM turbulent model and considering different sizes for calcium carbonate particles. The Eulerian-Lagrangian statistical approach was used to study the cyclone performance. The one-way and two-way coupling models were used and compared according to the results of cut-off size diameter and collection efficiency. Using two-way coupling, the contour plots of erosion flux are also depicted for the three configurations.

2. Conceptual design

The Stairmand cyclone consists of four parts, namely inlet channel, central cylinder, vortex finder, and the cone section (see Figure 1). The dimensions of these parts are listed in Table 1. One-inlet, two-inlet, and four-inlet configurations are presented in Figure 2. The two-phase flow of gas and calcium carbonate particles is blown through the cyclone inlet channel tangentially. The tangential velocity decreases when the flow moves down the cyclone until it reaches the cone section, where the decreasing trend of tangential velocity is inverted. In the cone section, where the second vortex formation happens, lighter particles are moved by the centrifugal force originated from tangential velocity towards the flow core, and they were ascended through the cyclone outlet.

The following assumptions were used in the present study:

- Mach number is equal to 0.06; therefore, the fluid flow can be considered incompressible (Parvaz et al., 2017).
- The temperature is constant and set to 300 K (Hoekstra, 2000).
- Particles are assumed spherical. Dust loading was considered as 0.0005 kg powder per the unit volume of air with a mean powder diameter of 5.97 μm and a geometric standard deviation of 2.08 (ANSYS Fluent User's Guide, 2013).
- Buoyancy and virtual mass forces were neglected (Zhao, 2005).
- Volumetric flow rate is constant and equal to $0.0839475\ \mathrm{m^3 s^{-1}}$.
- The inlet flow is uniform.

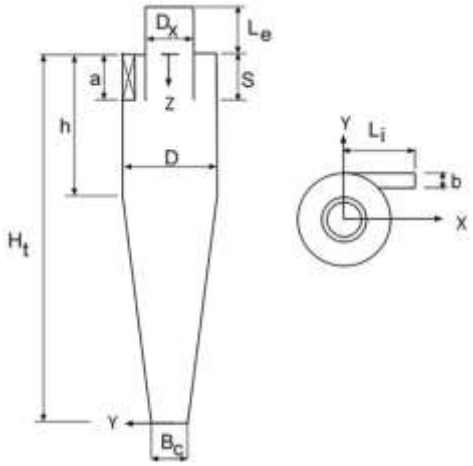

Figure 1
A schematic representation of Stairmand cyclone geometry.

Table 1
Geometrical properties of the investigated cyclone in the present work.

Parameters	D	a	b	D_x	S	B_c	h	H_t	L_e	L_i
Dimensional (m)	0.205	0.105	0.041	0.105	0.105	0.0768	0.3075	0.82	0.1025	0.1025
Non-dimensional	1	0.5121	0.2	0.5	0.5	0.375	1.5	4	0.5	0.5

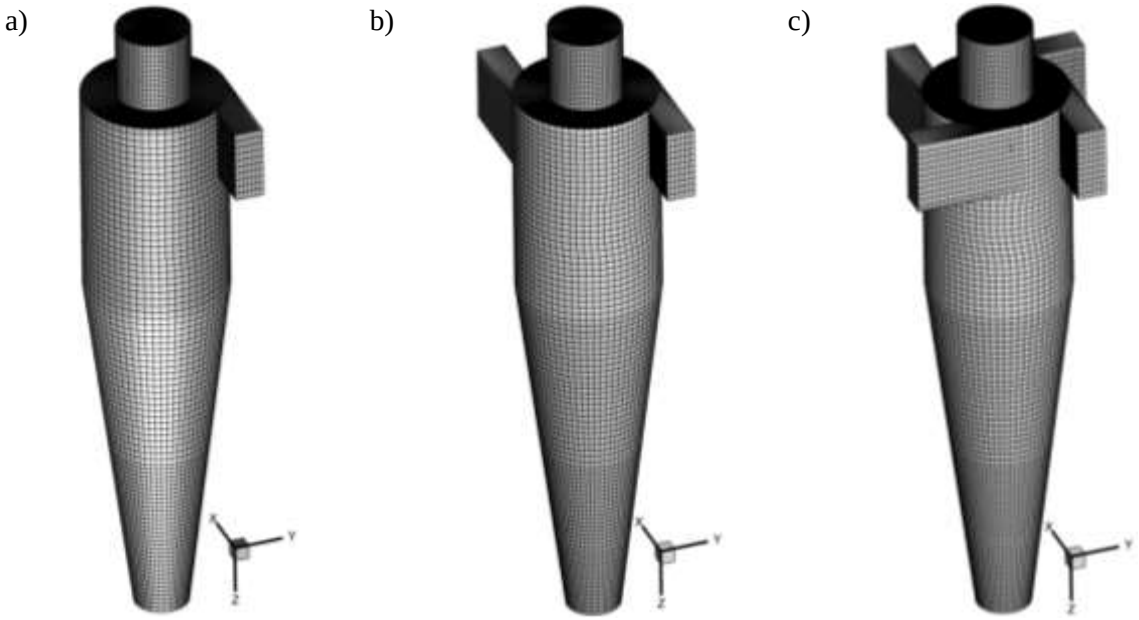

Figure 2
Representation of the generated mesh for a) one-inlet, b) two-inlet, and c) four-inlet configurations.

3. Governing equations

3.1. Eulerian equations-continuous phase

According to the assumptions, the continuity and momentum equations are as follows (Brar et al., 2015a).

$$\frac{\partial \overline{u_i}}{\partial x_i} = 0 \tag{1}$$

$$\frac{\partial \overline{u_i}}{\partial t} + \overline{u_j}\frac{\partial \overline{u_i}}{\partial x_j} = -\frac{1}{\rho}\frac{\partial p}{\partial x_i} + \nu\frac{\partial^2 \overline{u_i}}{\partial x_j \partial x_j} - \frac{\partial}{\partial x_j}R_{ij} + S_v \tag{2}$$

In above equations, $\overline{u_i}$ is mean velocity, and x_i is location; $\bar{p}$ stands for mean pressure and ρ is gas density; ν and $R_{ij}\left(=\overline{\acute{u}_i\acute{u}_j}\right)$ represent kinematic viscosity and Reynolds stress tensor respectively. The fluctuating component of fluid velocity (u') was considered as $u_i - \overline{u_i}$ (Kaya and Karagoz, 2009).

3.2. Turbulence closure-RSM

Taking the Reynolds stress tensor into account, the following equation was written (Hoekstra, 2000; Gao et al., 2013b; ANSYS Fluent User's Guide, 2013):

$$\begin{aligned}\frac{\partial}{\partial t}R_{ij} + \overline{u_k}\frac{\partial}{\partial x_k}R_{ij} &= \frac{\partial}{\partial x_k}\left(\frac{\nu_t}{\sigma^k}\frac{\partial}{\partial x_k}R_{ij}\right) - \left[R_{ik}\frac{\partial \overline{u_j}}{\partial x_k} + R_{jk}\frac{\partial \overline{u_i}}{\partial x_k}\right] - C_1\frac{\varepsilon}{k}\left[R_{ij} - \frac{2}{3}\delta_{ij}K\right] \\ &\quad - C_2\left[P_{ij} - \frac{2}{3}\delta_{ij}P\right] - \frac{2}{3}\delta_{ij}\varepsilon\end{aligned} \tag{3}$$

The turbulence generating terms are defined by:

$$P_{ij} = -\left[R_{ik}\frac{\partial \overline{u_j}}{\partial x_k} + R_{jk}\frac{\partial \overline{u_i}}{\partial x_k}\right], \qquad P = \frac{1}{2}P_{ij} \tag{4}$$

P indicates stress generation term, and ν_t is turbulent viscosity. $\sigma^k = 1$, $C_1 = 1.8$, and $C_2 = 0.6$ are empirical constants (Kaya and Karagoz, 2009; Hoekstra, 2000).

The transport equation for turbulence dissipation rate is given by:

$$\frac{\partial \varepsilon}{\partial t} + \overline{u_j}\frac{\partial \varepsilon}{\partial t} = \frac{\partial}{\partial x_j}\left[\left(\nu + \frac{\nu_l}{\sigma^\varepsilon}\right)\frac{\partial \varepsilon}{\partial x_j}\right] - C^{\varepsilon 1}\frac{\varepsilon}{K}R_{ij}\frac{\partial \overline{u_i}}{\partial x_j} - C^{\varepsilon 2}\frac{\varepsilon^2}{K} \tag{5}$$

where, $K\left(=\overline{\acute{u}_i\acute{u}_i}/2\right)$ is the turbulence kinetic energy, and ε represents the turbulence dissipation rate. The constants of Equation 5 are as follows: $\sigma^\varepsilon = 1.3$, $C^{\varepsilon 1} = 1.44$, and $C^{\varepsilon 2} = 1.92$ (Kaya and Karagoz, 2009; Hoekstra, 2000).

3.3. Lagrangian equations-dispersed phase

Only drag and gravitational forces are considered because of the lower density of air with respect to calcium carbonate. The momentum equations imposed on particles reads:

$$\frac{du_p}{dt} = F_D\left(\overline{u_g} + \acute{u}_g - u_p\right) - g \tag{6}$$

$$\frac{dv_p}{dt} = F_D\left(\overline{v_g} + \acute{v_g} - v_p\right) + \frac{w_p^2}{r_p} \tag{7}$$

$$\frac{dw_p}{dt} = F_D\left(\overline{w_g} + \acute{w_g} - w_p\right) - \frac{u_p w_p}{r_p} \tag{8}$$

in which, g and p indexes show the continuous (gas) and dispersed (particle) phases respectively. F_D represents the drag force defined by (Demir et al., 2016):

$$F_D = \frac{18\mu}{\rho_p d_p^2}\frac{C_D Re_p}{24} \tag{9}$$

The drag coefficient C_D can be written as follows:

$$C_D = \begin{cases} \dfrac{24}{Re_p}, & Re_p \le 1 \\ \dfrac{24\left(1 + 0.15Re_p^{0.687}\right)}{Re_p}, & 1 < Re_p \le 1000 \\ 0.44, & Re_p > 1000 \end{cases} \tag{10}$$

The particle Reynolds number is defined by (Parvaz et al., 2017; Demir et al., 2016):

$$Re_p = \frac{d_p \rho_g \left|\overrightarrow{\varphi_g} - \overrightarrow{\varphi_p}\right|}{\mu} \tag{11}$$

where, d_p is particle diameter; ρ_g, μ, and φ stand for density, dynamic viscosity, and all the components of the velocity of gas respectively.

3.4. Erosion model

Erosion occurred due to the impact of particles and the cyclone wall. The Det Norske Veritas (DNV) erosion model, known as the general erosion model, is used in this study. The three main steps of erosion prediction through CFD are flow modeling, particle tracking, and erosion calculation. RANS equations in addition to continuity and momentum transport equations are solved in an Eulerian framework to calculate the continuous flow field (ANSYS Fluent User's Guide, 2013). Newton's momentum equations are employed to track both the particle path and the particle velocity using two-way coupling with the continuous phase. The CFD-based erosion model for predicting the erosion rate is given by:

$$E = \dot{m}_p K f(\alpha)\left(\overrightarrow{\varphi_p}\right)^n \tag{12}$$

$$K = \frac{\pi^2}{2\sqrt{10}}\gamma^{2.5}\sqrt{\frac{1}{\rho_p}}\left[\frac{1 - q_p^2}{Y_p} - \frac{1 - q_w^2}{Y_w}\right]^2 \tag{13}$$

$$f(\alpha) = 2.4647 \times 10^{-3}\alpha + 2.9284 \times 10^{-4}\alpha^2 + 2.1974 \times 10^{-6}\alpha^3 \tag{14}$$

where, E, K, and $f(\alpha)$ are erosion rate, material constant, and the function of impact angle respectively. All the constants are expressed in the work done by Sedrez et al. (2017).

Two-way coupling is used for coupling the discrete and continuous phases. It considers the interactions between gas and particles. The source term, included in Equation 2, makes the coupling possible and is expressed by:

$$S_v = \sum_{i}^{np} \left[F_D \left(\overrightarrow{\varphi_g} - \overrightarrow{\varphi_p}^{i} \right) \right] \left(\dot{m}_p \Delta t \right) \tag{15}$$

in which, $F_D \left(\overrightarrow{\varphi_g} - \overrightarrow{\varphi_p}^{i} \right)$ shows the drag force imposed on particle i, and $\dot{m}_p$ indicates the overall mass flow rate of the particles. Δt is the time step set to 0.0001 s for all of the configurations. It is worth noting that the two-way coupling is just used for the investigation of the collection efficiency, cut-off size diameter, and erosion flux.

The resident time inside the cyclone can be calculated by the following relation (Parvaz et al., 2017).

$$t_{res} = \frac{V}{Q} \tag{16}$$

where, V is cyclone volume, and Q represents the volumetric flow rate. The resident time for all the configurations is tabulated in Table 2.

Table 2
The number of cells of the three configurations investigated in the present work.

Configuration	One-inlet	Two-inlet	Four-inlet
Volume (m^3)	0.0199	0.0203	0.0212
Resident time (s)	0.237	0.248	0.2527

3.5. Boundary conditions

The mixture of gas and particles, with given properties in Table 3, enters the cyclone at a uniform velocity yet tangentially through the inlet channels. The inlet velocities of one-inlet, two-inlet, and four-inlet configurations at a constant total volumetric mass flow rate are 19.5 ms^{-1}, 9.75 ms^{-1}, and 4.875 ms^{-1} respectively. The turbulence intensity and turbulent length are respectively 5% and 0.07 of the inlet width. The cyclone body is considered as wall, and the overflow at the top of the cyclone is defined as an outflow. The bottom of the cyclone is also considered as a trap to estimate the cyclone efficiency (Parvaz et al., 2017).

Table 3
Physical properties of air and calcium carbonate particles (Vahedi, et al, 2017a; Parvaz, et al. 2017).

Physical properties	Density (kgm^{-3})	Dynamic viscosity (Pa.s)
Air	1.225	0.00017694
Calcium carbonate	2740	-

4. Grid independence study and validation

It is important to perform a grid independence study before validation (Golshadi et al., 2013). Consequently, hexagonal cells were created via Gambit software as displayed in Figure 3. Achieving a good numerical simulation is undoubtedly originated from an accurate mesh generation. The multi-block hexahedral grids were produced in the current study for the whole domain of the cyclone. The two main features should be considered in the mesh generation; first, the grids should be generated in parallel to the flow direction in the entire computational domain. Second, the grid should be created so that they are capable of resolving the steep flow gradient in the central region of the cyclone due to the procession vortex core (PVC) phenomenon.

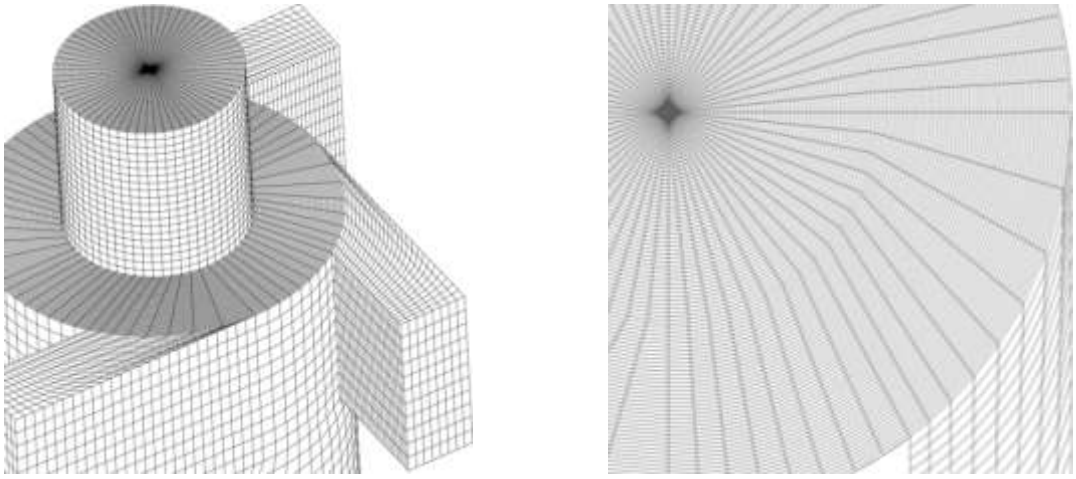

Figure 3
Two schematic representations of blocks and structured grid used in the simulation.

The simulations described here are run using ANSYS Fluent 16, Fluent Inc. The reference parameters for the mesh independence study are Euler number $\left(Eu = \rho u_{in}^2/2\right)$ and total pressure drop (the difference between the inlet and outlet static pressure). The number of cells is increased, and these parameters are analyzed as seen in Table 4, where the mesh independency is studied for one-inlet configuration.

After studying mesh independency, the results of the current simulation was validated by the experimental work done by Hoekstra (2000). Hence, a one-inlet cyclone (Figure 2a) was considered. The outcomes of the simulation of axial and tangential velocities at the distance of 0.9425 m from the bottom of the cyclone were compared to the experimental results of Hoekstra (2000). As it can be seen in Figure 4a, the tangential velocity profiles of these two studies show good agreement with an average deviation of 0.518% from Hoekstra's (2000) experimental result. It is worth noting that *x* and *y* directions were divided respectively by cylinder radius and inlet velocity to become dimensionless.

Table 4
The results of grid study for one-inlet channel.

Number of cells	Euler number	Total pressure drop
394700	5.8	1139.28
455900	6	1159.77
578300	6.2	1188.48
Percentage of deviation	0.064	4.1

Figure 4b illustrates the validation of the results of the dispersed phase. The results were compared to the experimental data released by Zhao (2005). It is clear that the dispersed phase could be simulated well with an average deviation of 16.6% from the results of Zhao (2005). The solid calcium carbonate particles were injected to the cyclone in the normal direction of inlet channel cross-section at the same velocity of air flow. To compute the efficiency of the cyclone, its bottom is considered as a trap. In the present study, the particle-wall collisions are considered elastic. Therefore, the coefficients of restitution in tangential as well as in wall normal direction are set to 1.

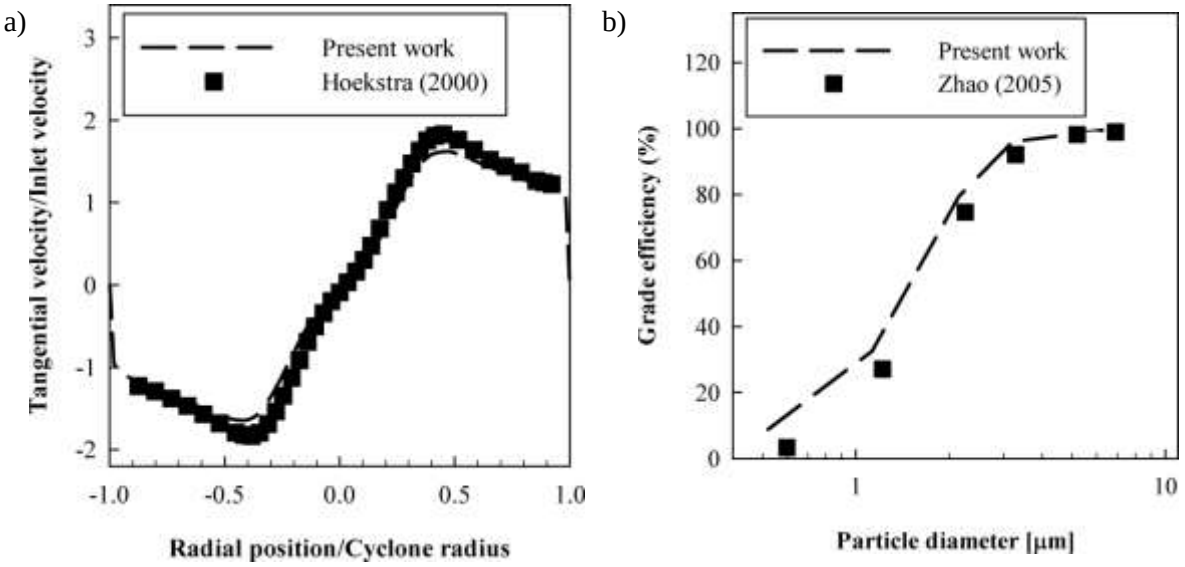

Figure 4
Comparison between a) tangential velocity and b) the dispersed phase of the current numerical simulation and the work done by Hoekstra (2000) and Zhao (2005).

5. Results and discussion

To study the flow pattern and the demonstration of tangential and axial velocity, which play important roles in separation, four sections were considered according to Table 5.

Table 5
Sections investigated for tangential and axial velocity distributions.

Situation	S_1	S_2	S_3	S_4
Z/D	0.75	1.5	2.25	2.75

5.1. Number of inlets and velocity components

Tangential and axial velocities are two important factors affecting the gas-particle cyclone performance; they have important roles in the separation process. The former causes centrifugal force, whereas the latter accounts for the transportation of particles down the cyclone (Elsayed and Lacor, 2012). The effects of inlet channel numbers on these velocity components of three configurations were investigated in the current numerical work at a constant total volumetric inlet mass flow rate. Figures 5-8 illustrate the tangential velocity in four sections mentioned in Table 5, and Figures 9-12 present the axial velocity in those sections.

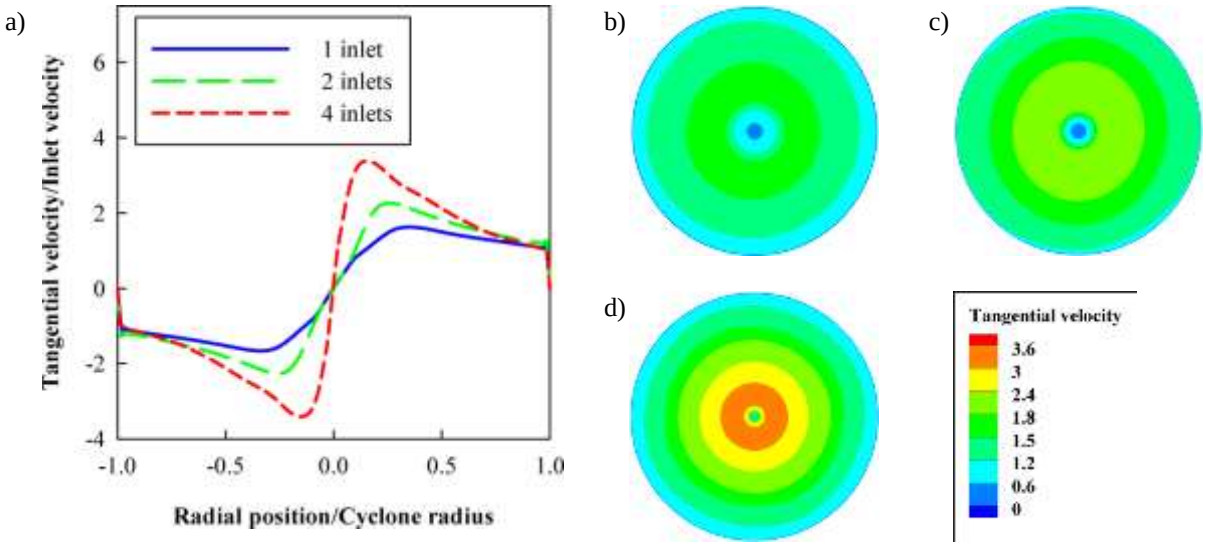

Figure 5
Normalized tangential velocity distribution in section S_1 a) for the three configurations and its contour plots for b) one-inlet, c) two-inlet, and d) four-inlet cyclone.

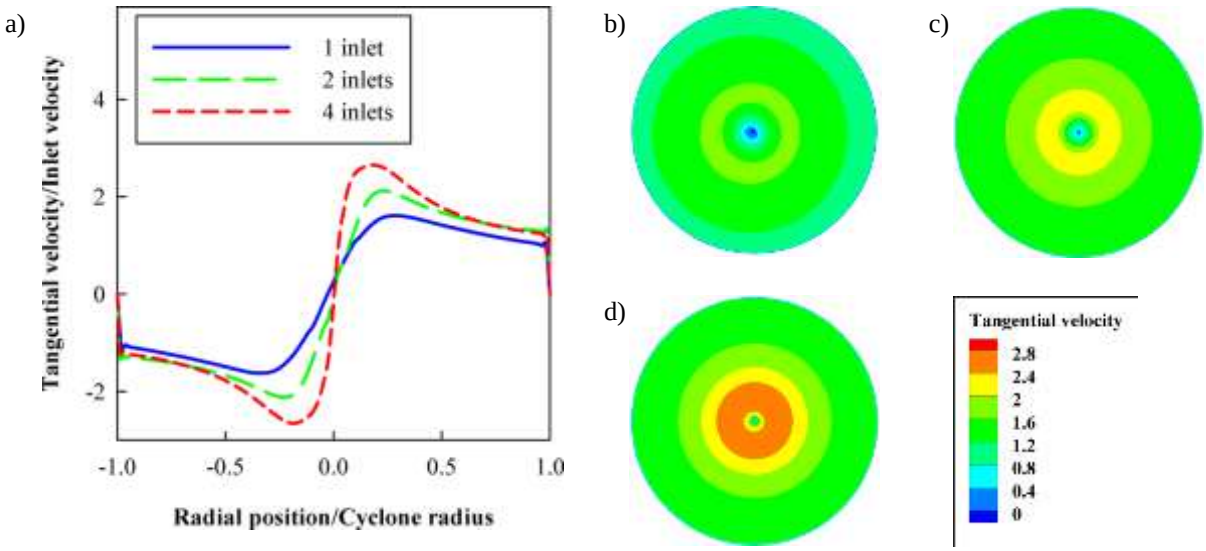

Figure 6
Normalized tangential velocity distribution in section S_2 a) for the three configurations and its contour plots for b) one-inlet, c) two-inlet, and d) four-inlet cyclone.

As it is shown in Figure 5, the profile of tangential velocity is almost centrally symmetric. The tangential velocity increases from wall to the center of the cyclone until it reaches its maximum at about 20% of the distance between the wall of the cyclone and its central axis. Then, the tangential velocity reaches 0 near the center of the cyclone. With an increase in the number of inlet channels, the tangential velocity in sections increases, and the maximum velocity takes place closer to the central axis of the cyclone. When the inlet numbers rises from 1 to 4, the maximum tangential velocity increases by 112.5%, 60.6%, 43.7%, and 43.7% for all the sections (from top to the bottom of the cyclone). The highest increase in tangential velocity occurs for the top section with a four-inlet configuration. It must be noted that one of the most important factors in increasing the Stairmand cyclone efficiency is the increase of tangential velocity (Avci and Karagoz, 2003; Demir et al., 2016).

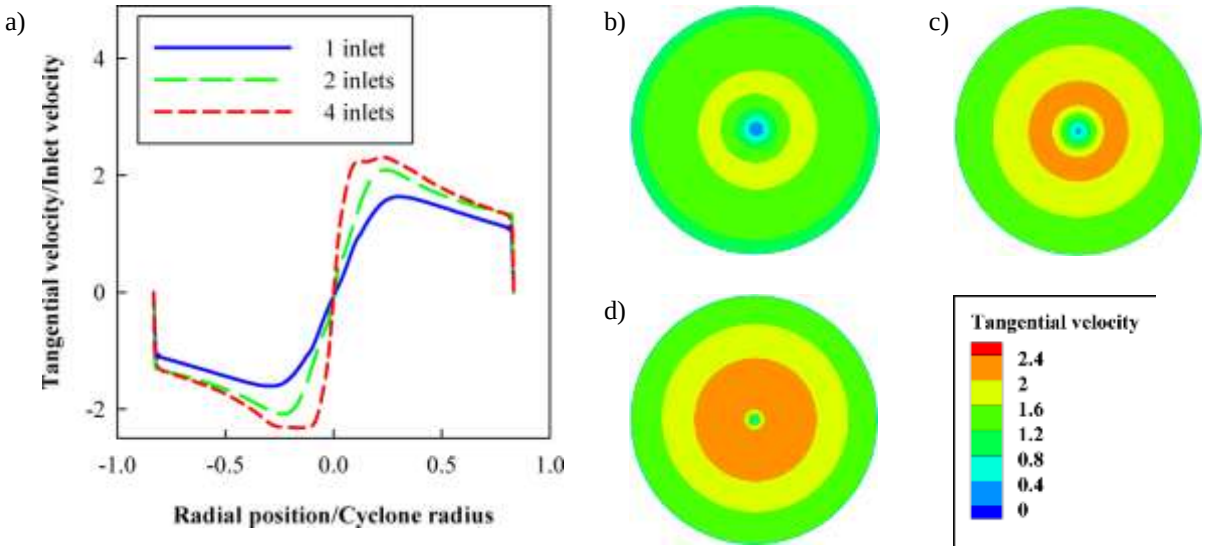

Figure 7
Normalized tangential velocity distribution in section S_3 a) for the three configurations and its contour plots for b) one-inlet, c) two-inlet, and d) four-inlet cyclone.

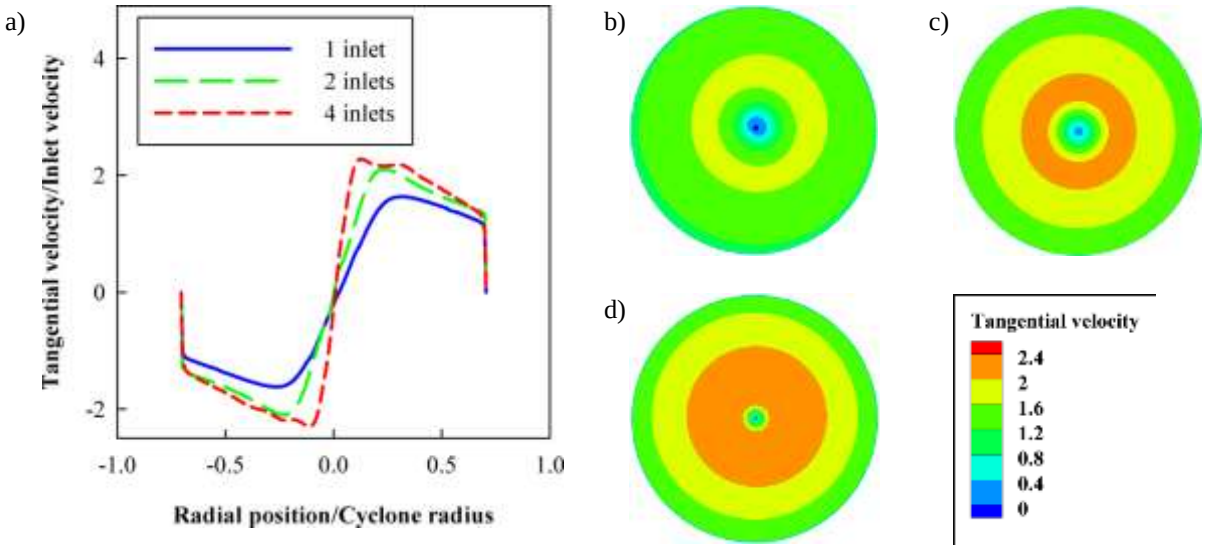

Figure 8
Normalized tangential velocity distribution in section S_4 a) for the three configurations and its contour plots for b) one-inlet, c) two-inlet, and d) four-inlet cyclone.

As it is obvious from Figures 5-8, the Rankine vortex region rises by increasing inlet numbers. The Rankine vortex and tangential velocity are two important parameters in the separation of particles and cyclone performance, so the results reveal a positive effect of adding inlets to the cyclone. According to these figures, the highest Rankine vortex region belongs to the four-inlet configuration.

The profiles and contour plots of axial velocity, which consists of upward and downward flows, are demonstrated in Figures 9-12 for different sections. Between the two upward and downward flows, the axial component of velocity becomes zero. Also, the axial velocity profiles are almost symmetric like tangential velocity profiles. Moving from wall to the center of the cyclone, the axial velocity increases from zero to its maximum. This component of velocity is very sensitive to the number of

inlets. For instance, in one-inlet and two-inlet configurations, the axial velocity value is negative at the center of the cyclones, and particles move downward, while, in four-inlet configuration, the axial velocity is positive at the center of the cyclones and transports the particles upward.

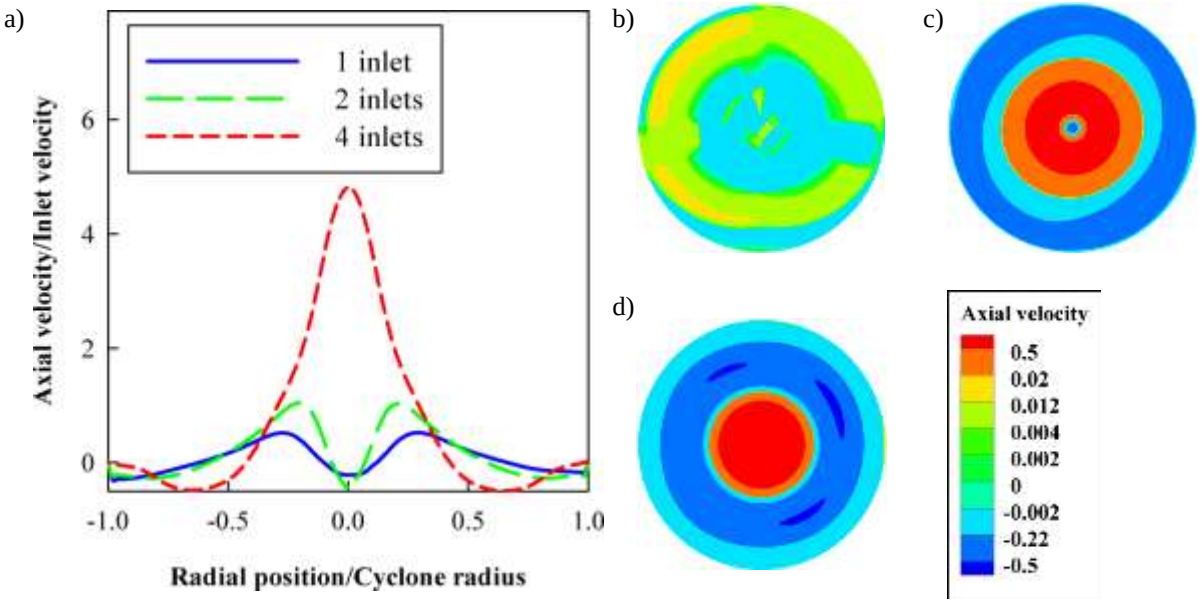

Figure 9
Normalized axial velocity distribution in section S_1 a) for the three configurations and its contour plots for b) one-inlet, c) two-inlet, and d) four-inlet cyclone.

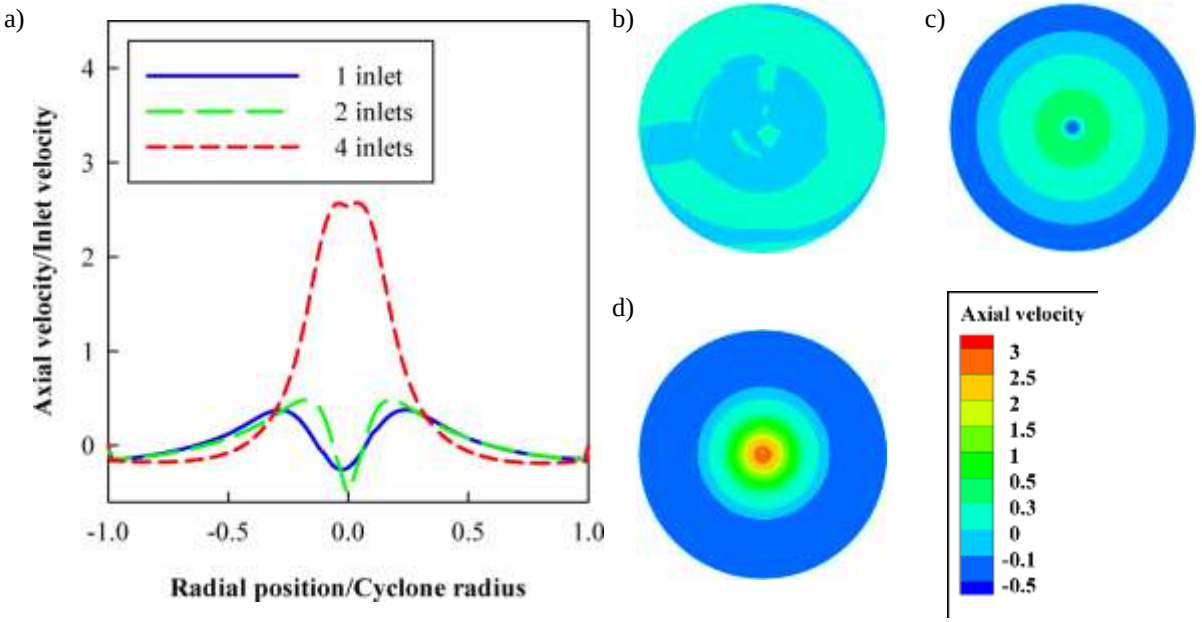

Figure 10
Normalized axial velocity distribution in section S_2 a) for the three configurations and its contour plots for b) one-inlet, c) two-inlet, and d) four-inlet cyclone.

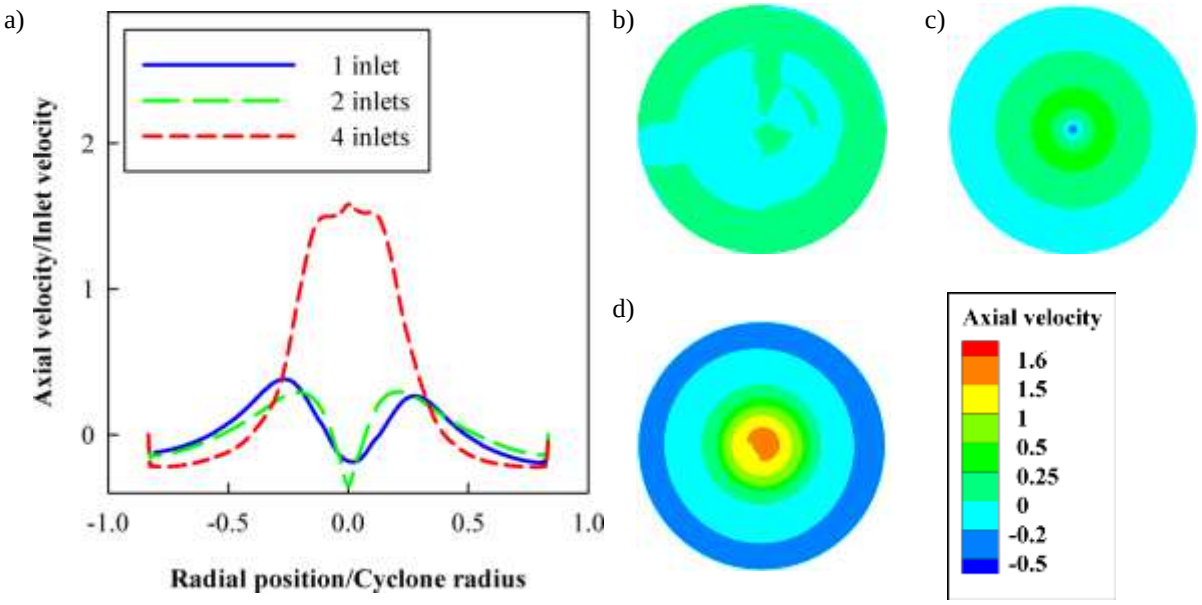

Figure 11
Normalized axial velocity distribution in section S_3 a) for the three configurations and its contour plots for b) one-inlet, c) two-inlet, and d) four-inlet cyclone.

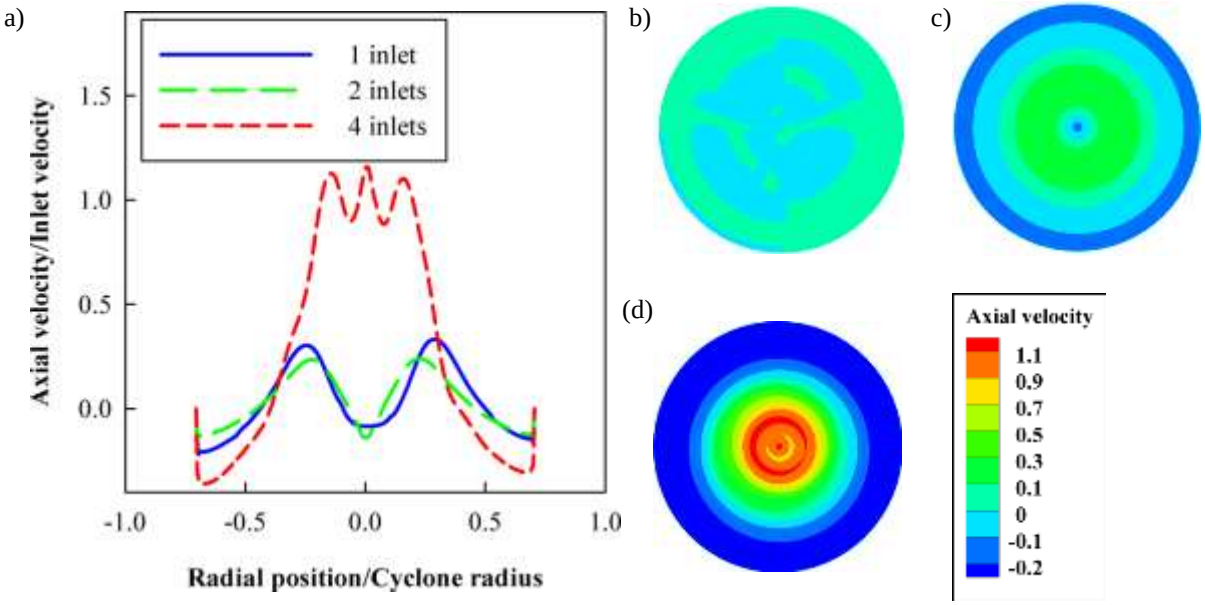

Figure 12
Normalized axial velocity distribution in section S_4 a) for the three configurations and its contour plots for b) one-inlet, c) two-inlet, and d) four-inlet cyclone.

It must be mentioned that the most important region for the separation process is the cylinder in which the two cross sections of S_1 and S_2 are located. Axial velocity is increased by adding extra inlet channels, but it declines by going down the cyclone. Furthermore, it can be seen that the area of the forced vortex is smaller in S_1 and S_2 sections compared to the other sections.

The downstream flow rate is a factor confirming that the axial velocity analyzing in the cyclone is inevitable. According to the sections of Figures 9-12, it is obvious that the downstream flow rate

improves by an increase in the number of inlet channels. Increasing downstream flow rate collects more particles at the bottom of the cyclone, thereby enhancing its efficiency.

5.2. Number of inlets and pressure drop

In gas-particle cyclones, the pressure drop is a result of the friction between gas and cyclone wall. The pressure drop distribution is very important in a cyclone, and it should not decrease because it may affect the cyclone performance in a negative manner. Generally, the relation between the velocity and pressure drop is defined by:

$$\Delta P = \xi \frac{\rho v_{in}^2}{2} \tag{17}$$

According to Figure 13, it is obvious that with an increase in the number of inlets, the pressure drop increments. On the other hand, the cyclone with four inlets experiences the lowest static pressure at its center.

5.3. Number of inlets and the cyclone efficiency

After investigating the velocity and pressure drop distributions, the efficiency of all the cyclone configurations is studied. The cyclones can be recognized by two important factors, namely the cyclone efficiency and the cut-off size diameter, which depends on cyclone geometry. The cut-off size is a criterion to evaluate the cyclone efficiency, and it shows the ability of cyclone in the separation of particles.

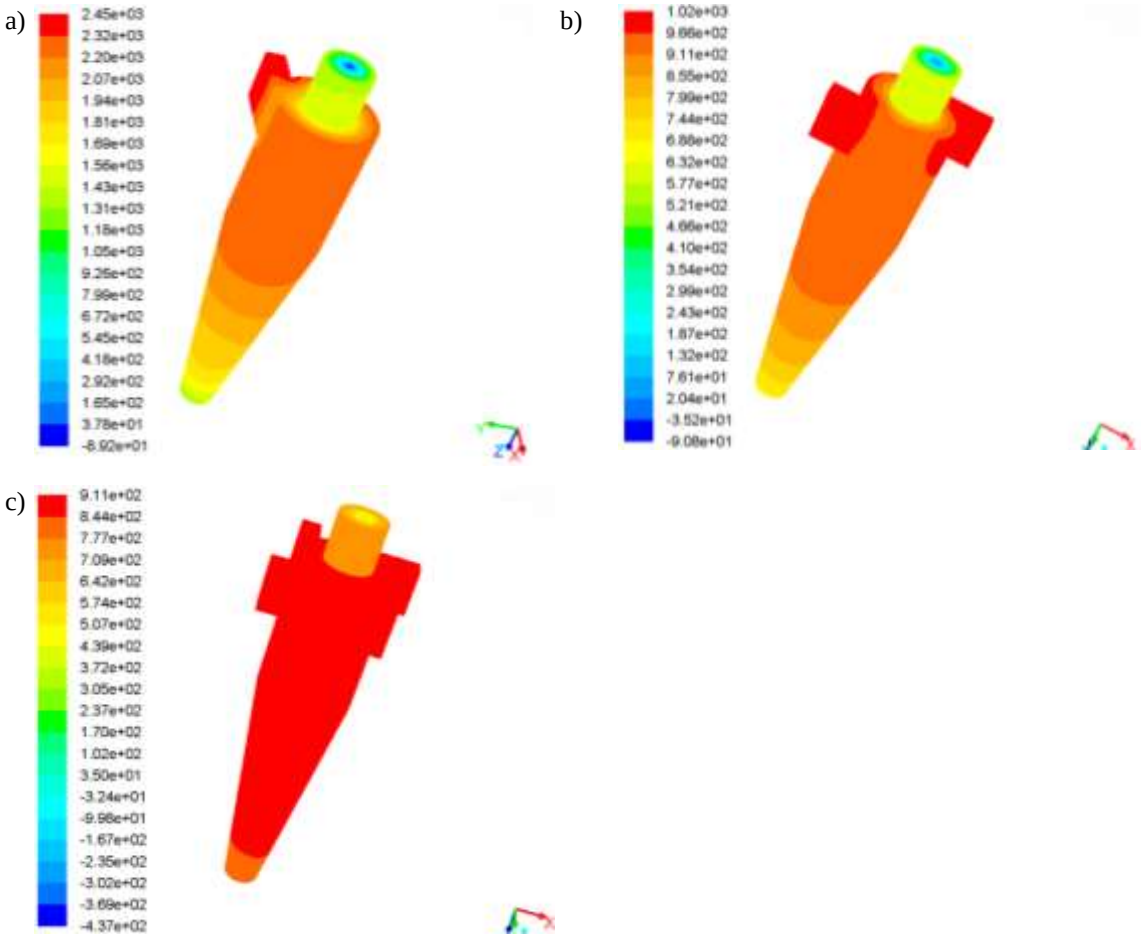

Figure 13
Pressure distribution throughout a) one-inlet, b) two-inlet, and c) four-inlet cyclones.

In Figure 14, the cyclone efficiency is displayed for different configurations and calcium carbonate particle sizes by considering one-way and two-way coupling models. Referring to this figure, the maximum cyclone efficiency is obtained when the cyclone has four inlets. On the other hand, with an increment in the particle size of calcium carbonate, the efficiency will rise. In addition, it can be seen that there is a little difference between cyclone efficiency for particle sizes less than 0.1 micrometers, while there is almost no difference in efficiency for all the configurations when the particle diameter equals 10 micrometers; the differences for the particles with a mid-range diameter are not predictable. Comparing Figures 14a and 14b, it is clear that there is no noticeable difference between the results of one-way and two-way coupling methods. However, the latter underestimates the cyclone efficiency.

The cut-off size is presented for the three configurations in Figure 15. It can be seen that the cut-off size diameter has a reverse relation with the number of inlets. The four-inlet cyclone has the smallest cut-off size diameter, which means that smaller particles are more susceptible to be collected. We experience a decline of 40% in cut-off size diameter in the four-inlet cyclone compared to the one-inlet cyclone. The physical explanation for this decline is the accumulation of large particles due to increased tangential velocity, which results in a shorter residence time and more particle collection. The one-way and two-way coupling methods were also compared in this figure to show their impacts on the cut-off size diameter. The two-way coupling method overestimates the cut-off size diameter, which leads to a decline in efficiency of the cyclone.

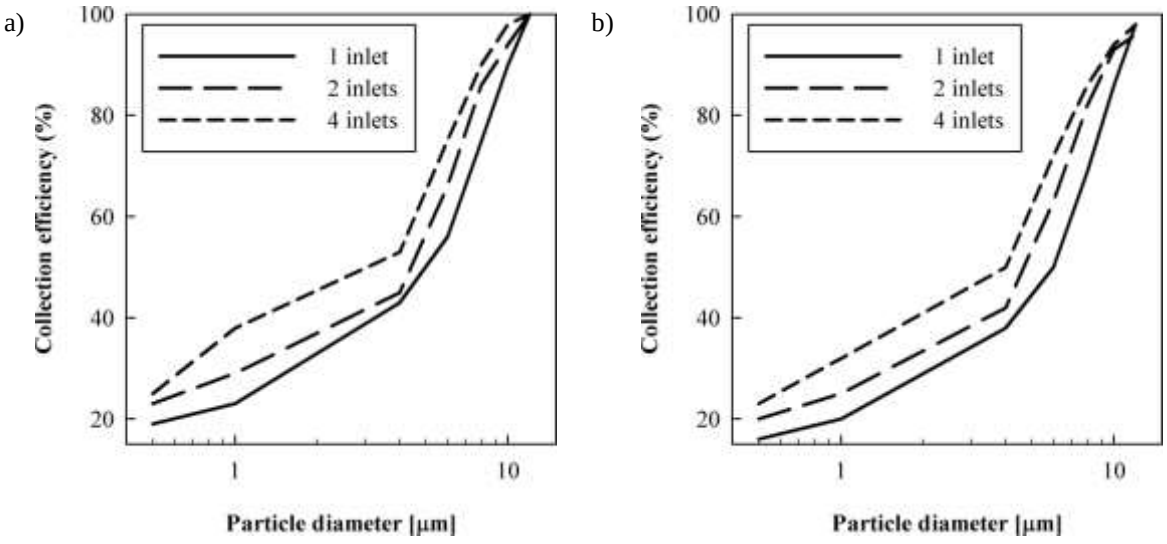

Figure 14
The collection efficiency for the three cyclone configurations for particle diameter in the range of 1 μm to 10 μm using a) one-way coupling and b) two-way coupling modeling.

5.4. Number of inlets and erosion

The main factors causing erosion are a high velocity and loading rate. Thus, the severely eroded locations experience a high velocity. As it can be seen in Figure 16, at a constant total volumetric mass flow rate, the inlet velocity of a typical cyclone is higher than that of two-inlet and four-inlet cyclones. Therefore, it can be stated that the erosion is much higher in a single-inlet cyclone compared to two-inlet and four-inlet configurations. It is also obvious that at the bottom of the cyclone, where there is an ascending flow at a high velocity, the erosion flux is critical.

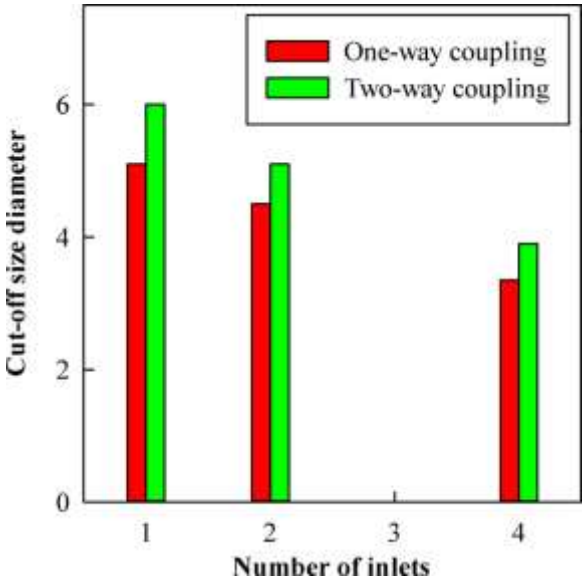

Figure 15
Cut-off size diameter magnitude for a) one-way coupling and b) two-way coupling modeling for the three cyclone configurations.

Although the flux of erosion specifies the location where erosion is most likely to happen, it is necessary, especially for industrialists, to classify cyclones with a mere value to better compare them. Therefore, by integrating the flux of erosion throughout the surfaces, the erosion rate is calculated at the specified volumetric flow rate. The same analysis was conducted at different volumetric flow rates to better analyze the effect of gas velocity on moving particles. The flow rates correspond to velocities in the range of 20 ms^{-1} to 45 ms^{-1} for the one-inlet configuration. As shown in Figure 13, the pressure has its lowest value in the four-inlet cyclone. Since the erosion is highly linked to pressure, as to velocity, the erosion experiences the lowest value in the four-inlet configuration. Moreover, Figure 17 clearly depicts that erosion is in direct relation to inlet velocity.

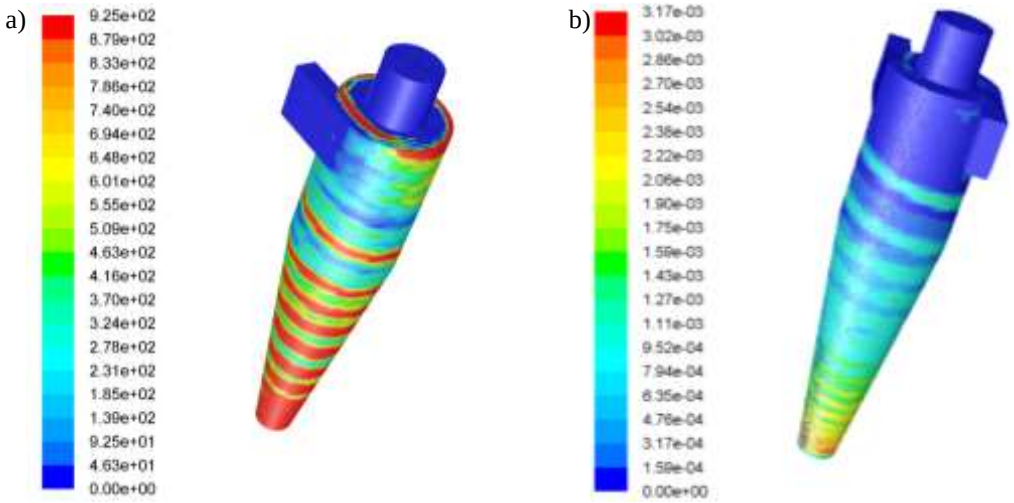

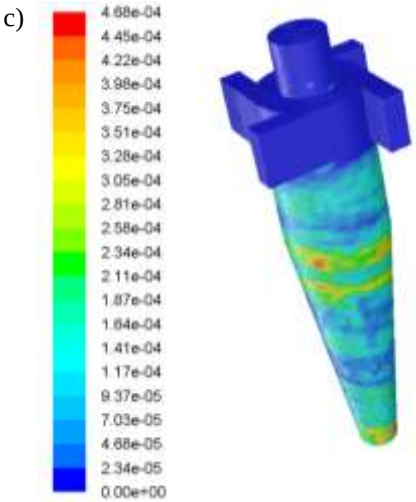

Figure 16
Erosion flux contours throughout a) one-inlet, b) two-inlet, and c) four-inlet cyclones.

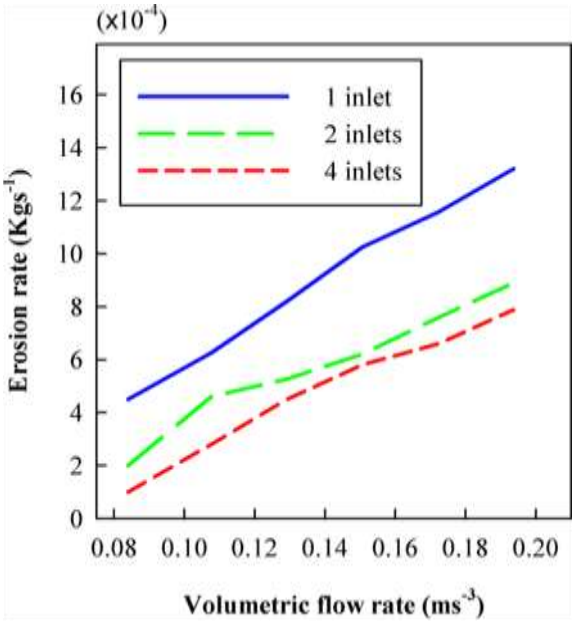

Figure 17
Erosion rate profiles for one-inlet, two-inlet, and four-inlet cyclones at different volumetric flow rates.

6. Conclusions

In the present study, the effects of adding inlets to the cyclone at a constant total volumetric mass flow rate and different particle sizes were studied. Reynolds stress model (RSM) was employed to simulate the turbulent flow of the continuum phase, while the Eulerian-Lagrangian approach was applied to particle tracking and cyclone performance investigation. The two-way coupling was used to investigate the gas-particle interaction and predict the locations which are susceptible to erosion. The results can be listed as follows:

- Adding three extra inlet channels to cyclone and dividing the total inlet mass flow rate over channel numbers increase the tangential velocity and lead to a larger Rankine vortex region.

- The axial velocity profile changes its shape from W-shape to jet flow by adding the inlet channels to the cyclone, which is an important indicator of efficiency. The four-inlet configuration intensifies the axial velocity, which transports particles to the collector section.
- Pressure drop is defined as the mean pressure difference between the outlet and inlet static pressure. According to pressure contour plots in the current study, the four-inlet configuration accounted for the highest pressure drop.
- Cyclones can be distinguished by their efficiency; based on this study, adding inlet channels to the cyclone enhances the effect of centrifugal force on particles, which leads to a drop in cut-off size diameter and an improvement in efficiency.
- The bottom of cyclones and the surface in front of particle entrance are more susceptible to erosion than other parts. Additionally, the erosion flux is much lower in four-inlet configuration.
- The erosion rate increases monotonically by a rise in the inlet velocity and the pressure of the cyclone.

Nomenclature

C_D	: Drag coefficient
D	: Cyclone diameter
F_D	: Friction factor (kgm s^{-2})
g	: Gravitational acceleration (m s^{-2})
K	: Turbulence kinetics energy (kgm^2 s^{-2})
$\bar{p}$	: Mean pressure (Pa)
P	: Stress generation (kgm^{-1} s^{-2})
Q	: Volumetric flow rate (m^3 s^{-1})
R_{ij}	: Reynolds stress tensor
S_i	: Section of study (m)
t_{res}	: Particle residence time (s)
u	: *x*-component of velocity (m s^{-1})
u'	: Fluctuating component of velocity (m s^{-1})
$\bar{u}$	: Mean velocity (m s^{-1})
v	: *y*-component of velocity (m s^{-1})
V	: Cyclone volume (m^3)
w	: *z*-component of velocity (m s^{-1})
x_i	: Location (m)

Greek Symbols	
ε	: Turbulence dissipation
μ	: Dynamic viscosity (Pa s)
ν	: Kinematic viscosity ($m^2\ s^{-1}$)
ν_t	: Turbulent viscosity ($m^2\ s^{-1}$)
ρ	: Density ($kg\ m^{-3}$)
Subscripts	
p	: Particle
t	: Turbulence

References

Ansys Fluent User's Guide, Ansys Inc., Southpointe, Canonsburg, Pa, Usa, 2013.

Avci A. and Karagoz I., Effects of Flow and Geometrical Parameters on the Collection Efficiency in Cyclone Separators, Journal of Aerosol Science, Vol. 34, No. 7, p. 937-955, 2003.

Azadi M., Azadi M., and Mohebbi A., A CFD Study of the Effect of Cyclone Size on its Performance Parameters, Journal of Hazardous Materials, Vol. 182, No. 1, p. 835–841, 2010.

Brar, L. S., Sharma, R.P., and Elsayed, Kh., The Effect of the Cyclone Length on the Performance of Stairmand High-efficiency Cyclone, Powder Technology, Vol. 286, p. 668-677, 2015a.

Brar, L. S. and Sharma, R. P., Effect of Varying Diameter on the Performance of Industrial Scale Gas Cyclone Dust Separators, Materials Today: Proceedings, Vol. 2, p. 3230–3237, 2015b.

Chuah, T. G., Gimbun J., and Choong T. S., A CFD Study of the Effect of Cone Dimensions on Sampling Aerocyclones Performance and Hydrodynamics, Powder Technology, Vol. 162, No. 2, p. 126-132, 2006.

Demir, S., Karadeniz, A., and Aksel, M., Effects of Cylindrical and Conical Heights on Pressure and Velocity Fields in Cyclones, Powder Technology, p. 295, 209–217, 2016.

Elsayed, K. and Lacor, C., The Effect of the Dust Outlet Geometry on the Performance and Hydrodynamics of Gas Cyclones, Computational Fluids, Vol. 68, P. 134–147, 2012.

Gao X., Chen J., Feng J., and Peng X., Numerical Investigation of the Effects of the Central Channel on the Flow Field in an Oil–gas Cyclone Separator, Computers & Fluids, Vol. 92, p. 45–55, 2013a.

Gao, X., Chen, J., Feng, J., and Peng, X., Numerical and Experimental Investigations of the Effects of the Breakup of Oil Droplets on the Performance of Oil–gas Cyclone Separators in Oil-injected Compressor Systems, International Journal of Refrigeration, Vol. 36, No. 7, p. 1894–1904, 2013b.

Golshadi, M., Mosayebi Behbahani, R., and Irani, M., CFD Simulation of Dimethyl Ether Synthesis from Methanol in an Adiabatic Fixed Bed Reactor, Iranian Journal of Oil & Gas Science and Technology (Ijogst), Vol. 2, No. 2, p. 50–64, 2013.

Griffiths W. D. and Boysan F., Computational Fluid Dynamics (CFD) and Empirical Modelling of the Performance of a Number of Cyclone Samplers, Journal of Aerosol Science, Vol. 27, No. 2, p.

281-304, 1996.

Hoekstra, A. J., Gas Flow Field and Collection Efficiency of Cyclone Separators, Ph.D. Thesis, Delft University of Technology, Netherland, 2000.

Hosseini, S. M., Shahbazi, Kh., and Khosravi Nikou, M. R., A CFD Simulation of the Parameters Affecting the Performance of Downhole Deoiling Hydrocyclone, Iranian Journal of Oil & Gas Science and Technology (Ijogst), Vol. 4, No. 3, p. 77–93, 2015.

Iozia D. L. and Leith D., The Logistic Function and Cyclone Fractional Efficiency, Aerosol Science and Technology, Vol. 12, No. 3, p. 598-606, 1990.

Karagoz I., Avci A., Surmen A., and Sendogan O., Design and Performance Evaluation of a New Cyclone Separator, Journal of Aerosol Science, Vol. 59, p. 57–64, 2013.

Kaya F. and Karagoz I., Numerical Investigation of Performance Characteristics of a Cyclone Prolonged with a Dipleg, Chemical Engineering Journal, Vol. 151, No. 1, p. 39-45, 2009.

Mothes H. and Löffler F., Prediction of Particle Removal in Cyclone Separators, International Chemical Engineering, Vol. 28, No. 2, p. 231-240, 1988.

Nikou, M. K. and Ehsani, M. R., Turbulence Models Application on CFD Simulation of Hydrodynamics, Heat and Mass Transfer in a Structured Packing, International Communications in Heat and Mass Transfer, Vol. 35, No. 9, p.1211-1219, 2008.

Parvaz, F., Hosseini, S. H., Ahmadi, G., and Elsayed, Kh., Impacts of the Vortex Finder Eccentricity on the Flow Pattern and Performance of a Gas Cyclone, Separation and Purification Technology, Vol. 187, p. 1-13, 2017.

Vahedi, S. M., Parvaz, F., Rafee, R., and Khandan Bakavoli, M., CFD Simulation of Flow Pattern and Performance for a Conventional and a Dual-cone Gas-particle Cyclone, Journal of Heat and Mass Transfer Research (Jhmtr), Doi: 10.22075/Jhmtr.2017.11918.1170, 2017a.

Vahedi, S. M., Parvaz, F., and Khandan Bakavoli, M., Surface Roughness Effect of on Vortex Length and Efficiency of the Gas-oil Cyclone through CFD Modelling, Iranian Journal of Oil & Gas Science and Technology (ijogst), Doi: 10.22050/Ijogst.2018.102377.1417, 2017b.

Wang L., Feng J., Gao X., and Peng X., Investigation on the Oil–Gas Separation Efficiency Considering Oil Droplets Breakup and Collision in a Swirling Flow, Chemical Engineering Research and Design, Vol. 117, p. 394–400, 2017.

Zhao B., Su Y., and Zhang J., Simulation of Gas Flow Pattern and Separation Efficiency in Cyclone with Conventional Single and Spiral Double Inlet Configuration, Chemical Engineering Research and Design, Vol. 84, No. 12, p. 1158–1165, 2006.

Zhao B., Development of a New Method for Evaluating Cyclone Efficiency, Chemical Engineering and Processing: Process Intensification, Vol. 44, No. 4, p. 447–451, 2005.